Rotational dynamics of optically trapped nanofibers

Antonio Alvaro Ranha Neves,[1,*] Andrea Camposeo,[1] Stefano Pagliara,[2] Rosalba Saija,[3] Ferdinando Borghese,[3] Paolo Denti,[3] Maria Antonia Iatì,[4] Roberto Cingolani,[1] Onofrio M. Maragò,[4] and Dario Pisignano[1,2]

[1] *National Nanotechnology Laboratory of CNR-INFM, IIT Research Unit, Università del Salento, via Arnesano, 73100, Lecce, Italy.*
[2] *Scuola Superiore ISUFI, Università del Salento, via Arnesano, 73100, Lecce, Italy.*
[3] *Dipartimento di Fisica della Materia e Ingegneria Elettronica, Università di Messina, Salita Sperone 31, 98166 Messina, Italy.*
[4] *Istituto per i Processi Chimico-Fisici (sez. Messina), CNR, Salita Sperone, 98158 Faro Superiore, Messina, Italy.*
antonio.neves@unisalento.it

Abstract: We report on the experimental evidence of tilted polymer nanofiber rotation, using a highly focused linear polarized Gaussian beam. Torque is controlled by varying trapping power or fiber tilt angle. This suggests an alternative strategy to previously reported approaches for the rotation of nano-objects, to test fundamental theoretical aspects. We compare experimental rotation frequencies to calculations based on T-Matrix formalism, which accurately reproduces measured data, thus providing a comprehensive description of trapping and rotation dynamics of the linear nanostructures.

OCIS codes: (350.4855) Optical tweezers or optical manipulation; (170.4520) Optical confinement and manipulation; (170.0180) Microscopy; (290.5825) Scattering theory; (160.4236) Nanomaterials; (160.5470) Polymers.

References and links

1. K. Dholakia, P. Reece, and M. Gu, "Optical micromanipulation," Chem. Soc. Rev. **37**(1), 42–55 (2007).
2. J. R. Moffitt, Y. R. Chemla, S. B. Smith, and C. Bustamante, "Recent advances in optical tweezers," Annu. Rev. Biochem. **77**(1), 205–228 (2008).
3. A. Jonáš, and P. Zemánek, "Light at work: The use of optical forces for particle manipulation, sorting, and analysis," Electrophoresis **29**(24), 4813–4851 (2008).
4. N. B. Simpson, K. Dholakia, L. Allen, and M. J. Padgett, "Mechanical equivalence of spin and orbital angular momentum of light: an optical spanner," Opt. Lett. **22**(1), 52–54 (1997).
5. M. Padgett, and L. Allen, "Light with a twist in its tail," Contemp. Phys. **41**(5), 275–285 (2000).
6. H. He, M. E. J. Friese, N. R. Heckenberg, and H. Rubinsztein-Dunlop, "Direct observation of transfer of angular momentum to absorptive particles from a laser beam with a phase singularity," Phys. Rev. Lett. **75**(5), 826–829 (1995).
7. H. Polaert, G. Gréhan, and G. Gouesbet, "Forces and torques exerted on a multilayered spherical particle by a focused Gaussian beam," Opt. Commun. **155**(1-3), 169–179 (1998).
8. M. E. J. Friese, T. A. Nieminen, N. R. Heckenberg, and H. Rubinsztein-Dunlop, "Optical torque controlled by elliptical polarization," Opt. Lett. **23**(1), 1–3 (1998).
9. E. Higurashi, R. Sawada, and T. Ito, "Optically induced angular alignment of trapped birefringent micro-objects by linearly polarized light," Phys. Rev. E Stat. Phys. Plasmas Fluids Relat. Interdiscip. Topics **59**(3), 3676–3681 (1999).
10. A. I. Bishop, T. A. Nieminen, N. R. Heckenberg, and H. Rubinsztein-Dunlop, "Optical application and measurement of torque on microparticles of isotropic nonabsorbing material," Phys. Rev. A **68**(3), 033802 (2003).
11. K. D. Bonin, B. Kourmanov, and T. G. Walker, "Light torque nanocontrol, nanomotors and nanorockers," Opt. Express **10**(19), 984–989 (2002).
12. P. Galajda, and P. Ormos, "Orientation of flat particles in optical tweezers by linearly polarized light," Opt. Express **11**(5), 446–451 (2003).
13. E. Santamato, A. Sasso, B. Piccirillo, and A. Vella, "Optical angular momentum transfer to transparent isotropic particles using laser beam carrying zero average angular momentum," Opt. Express **10**(17), 871–878 (2002).
14. L. Paterson, M. P. MacDonald, J. Arlt, W. Sibbett, P. E. Bryant, and K. Dholakia, "Controlled rotation of optically trapped microscopic particles," Science **292**(5518), 912–914 (2001).

#117041 - $15.00 USD Received 11 Sep 2009; revised 19 Oct 2009; accepted 28 Oct 2009; published 6 Jan 2010

15. A. T. O'Neil, and M. J. Padgett, "Rotational control within optical tweezers by use of a rotating aperture," Opt. Lett. **27**(9), 743–745 (2002).
16. S. Sato, M. Ishigure, and H. Inaba, "Optical trapping and rotational manipulation of microscopic particles and biological cells using higher-order mode Nd:YAG laser beam," Electron. Lett. **27**(20), 1831–1832 (1991).
17. P. Galajda, and P. Ormos, "Complex micromachines produced and driven by light," Appl. Phys. Lett. **78**(2), 249–251 (2001).
18. E. Higurashi, R. Sawada, and T. Ito, "Optically induced rotation of a trapped micro-object about an axis perpendicular to the laser beam axis," Appl. Phys. Lett. **72**(23), 2951–2953 (1998).
19. E. Higurashi, H. Ukita, H. Tanaka, and O. Ohguchi, "Optically induced rotation of anisotropic micro-objects fabricated by surface micromachining," Appl. Phys. Lett. **64**(17), 2209–2210 (1994).
20. R. C. Gauthier, "Optical levitation and trapping of a micro-optic inclined end-surface cylindrical spinner," Appl. Opt. **40**(12), 1961–1973 (2001).
21. Y. Nakayama, P. J. Pauzauskie, A. Radenovic, R. M. Onorato, R. J. Saykally, J. Liphardt, and P. Yang, "Tunable nanowire nonlinear optical probe," Nature **447**(7148), 1098–1101 (2007).
22. O. M. Maragò, P. H. Jones, F. Bonaccorso, V. Scardaci, P. G. Gucciardi, A. G. Rozhin, and A. C. Ferrari, "Femtonewton force sensing with optically trapped nanotubes," Nano Lett. **8**(10), 3211–3216 (2008).
23. F. Di Benedetto, A. Camposeo, S. Pagliara, E. Mele, L. Persano, R. Stabile, R. Cingolani, and D. Pisignano, "Patterning of light-emitting conjugated polymer nanofibres," Nat. Nanotechnol. **3**(10), 614–619 (2008).
24. A. Camposeo, F. Di Benedetto, R. Stabile, A. A. R. Neves, R. Cingolani, and D. Pisignano, "Laser emission from electrospun polymer nanofibers," Small **5**(5), 562–566 (2009).
25. J. M. Moran-Mirabal, J. D. Slinker, J. A. DeFranco, S. S. Verbridge, R. Ilic, S. Flores-Torres, H. Abruña, G. G. Malliaras, and H. G. Craighead, "Electrospun light-emitting nanofibers," Nano Lett. **7**(2), 458–463 (2007).
26. N. J. Pinto, A. T. Johnson, A. G. MacDiarmid, C. H. Mueller, N. Theofylaktos, D. C. Robinson, and F. A. Miranda, "Electrospun polyaniline/polyethylene oxide nanofiber field-effect transistor," Appl. Phys. Lett. **83**(20), 4244–4246 (2003).
27. S. J. Parkin, G. Knöner, T. A. Nieminen, N. R. Heckenberg, and H. Rubinsztein-Dunlop, "Picoliter viscometry using optically rotated particles," Phys. Rev. E Stat. Nonlin. Soft Matter Phys. **76**, 041507 (2007).
28. J. Leach, H. Mushfique, R. di Leonardo, M. Padgett, and J. Cooper, "An optically driven pump for microfluidics," Lab Chip **6**(6), 735–739 (2006).
29. F. Borghese, P. Denti, and R. Saija, *Scattering from model nonspherical particles* (Springer, Berlin, 2007), 2nd ed.
30. J. A. Lock, "Calculation of the radiation trapping force for laser tweezers by use of generalized Lorenz-Mie theory. I. Localized model description of an on-axis tightly focused laser beam with spherical aberration," Appl. Opt. **43**(12), 2532–2544 (2004).
31. J. A. Lock, "Calculation of the radiation trapping force for laser tweezers by use of generalized Lorenz-Mie theory. II. On-axis trapping force," Appl. Opt. **43**(12), 2545–2554 (2004).
32. J. A. Lock, S. Y. Wrbanek, and K. E. Weiland, "Scattering of a tightly focused beam by an optically trapped particle," Appl. Opt. **45**(15), 3634–3645 (2006).
33. A. A. R. Neves, A. Fontes, C. L. Cesar, A. Camposeo, R. Cingolani, and D. Pisignano, "Axial optical trapping efficiency through a dielectric interface," Phys. Rev. E Stat. Nonlin. Soft Matter Phys. **76**, 061917 (2007).
34. F. Borghese, P. Denti, R. Saija, and M. A. Iatì, "Optical trapping of nonspherical particles in the T-matrix formalism," Opt. Express **15,** 11984–11998 (2007); **15**, 14618-14618 (2007). http://www.opticsinfobase.org/abstract.cfm?&id=141215
35. F. Borghese, P. Denti, R. Saija, M. A. Iatì, and O. M. Maragò, "Radiation torque and force on optically trapped linear nanostructures," Phys. Rev. Lett. **100**(16), 163903 (2008).
36. F. Borghese, P. Denti, R. Saija, and M. A. Iatì, "Radiation torque on nonspherical particles in the transition matrix formalism," Opt. Express **14**(20), 9508–9521 (2006).
37. B. Richards, and E. Wolf, "Electromagnetic Diffraction in Optical Systems. II. Structure of the Image Field in an Aplanatic System," Proc. R. Soc. Lond. A Math. Phys. Sci. **253**(1274), 358–379 (1959).
38. L. Novotny, and B. Hecht, *Principles of Nano-Optics* (Cambridge University Press, New York, 2006).
39. S. Broersma, "Viscous force and torque constants for a cylinder," J. Chem. Phys. **74**(12), 6989–6990 (1981).
40. D. Li, and Y. Xia, "Electrospinning of Nanofibers: Reinventing the Wheel?" Adv. Mater. **16**(14), 1151–1170 (2004).
41. D. H. Reneker, and I. Chun, "Nanometre diameter fibres of polymer, produced by electrospinning," Nanotechnology **7**(3), 216–223 (1996).
42. A. A. R. Neves, A. Fontes, L. Y. Pozzo, A. A. de Thomaz, E. Chillce, E. Rodriguez, L. C. Barbosa, and C. L. Cesar, "Electromagnetic forces for an arbitrary optical trapping of a spherical dielectric," Opt. Express **14**(26), 13101–13106 (2006).
43. K. Berg-Sørensen, and H. Flyvbjerg, "Power spectrum analysis for optical tweezers," Rev. Sci. Instrum. **75**(3), 594–612 (2004).
44. P. J. Pauzauskie, A. Radenovic, E. Trepagnier, H. Shroff, P. Yang, and J. Liphardt, "Optical trapping and integration of semiconductor nanowire assemblies in water," Nat. Mater. **5**(2), 97–101 (2006).
45. F. Xu, J. A. Lock, G. Gouesbet, and C. Tropea, "Radiation torque exerted on a spheroid: Analytical solution," Phys. Rev. A **78**(1), 013843 (2008).

#117041 - $15.00 USD Received 11 Sep 2009; revised 19 Oct 2009; accepted 28 Oct 2009; published 6 Jan 2010

1. Introduction

Optical forces are currently employed to study a range of chemical, physical and biological problems, by trapping microscale objects and measuring sub pico-Newton forces [1–3]. On optically trapped objects, the mechanisms for rotating consist in exploiting the physical properties of the trapping beam, the trapped object or both. A laser beam can carry intrinsic (spin) or extrinsic (orbital) angular momentum, associated to the polarization and to the light beam phase structure, respectively [4–7]. Either trapping beams with elliptical polarization or with a rotating linear polarization can be exploited to apply a torque to trapped objects [8–12]. Rotation of trapped particles can also be induced by exploiting the phase structure (such as Laguerre-Gaussian or Bessel beams) or by modifying the spatial intensity profile of the trapping focal spot [13–16]. The rotatable object can be spherical, exhibiting a birefringence or a slight absorption, or it can have more complex shapes, as in microfabricated propellers by two-photon polymerization [17–19] or cylinders with inclined faces [20].

In particular, optical trapping of elongated nanoparticles, including nanowires [21] and nanotubes [22], is gaining an increasing interest because of the high shape anisotropy and unique physical properties of these systems. Among linear nanostructures, nanofibers are novel materials with many strategic applications ranging from scaffolding for tissue-engineering to integrated photonics [23,24] and electronics [25,26]. Nevertheless, optical trapping and manipulation of polymer nanofibers is not studied in depth, despite understanding the optical forces and torques acting on these objects, as well as their trapping dynamics, might open new applications, exploiting the polymeric fibers as local probes or active elements in microrheology [27] and microfluidics [28], and in next generation Photonic Force Microscopy [21]. Furthermore, the nanofibers, possibly characterized by subwavelength diameters and lengths in the range 10-100 μm, constitute ideal systems for studying effects occurring in the intermediate regime between the Rayleigh scattering and geometrical optics.

Present methods used to rotate nano- and micro-objects require the manipulation of the beam profile or polarization, thus being scarcely efficient due to power loss in the process. Moreover, the trapped object needs to be slightly absorptive, birefringent, or specifically microfabricated. These restrictions are here avoided by a strategy to rotate a dielectric cylinder with flat end faces, based on a non-rotating linear polarized Gaussian (TEM_{00}) beam, carrying neither intrinsic nor extrinsic angular momentum. This enables a detailed analysis of the torque acting on fibers, whose experimental results are compared with calculations of optical trapping and rotation of linear nanostructures through a full electromagnetic theory.

2. Theory

2.1 Radiation force and torque

Light forces are generated by the scattering of electromagnetic fields incident on a particle, hence the quantitative understanding of optical trapping has to rely on the scattering theory of electromagnetic radiation [29–33]. The difficulties arising from the use of the full scattering theory are generally overcome by solving the problem in different regimes depending on the size of the scatterer. Moreover the models traditionally used for calculating optical forces are based on approximations which often limit the discussion only to spherical particles. On the contrary, in order to calculate the radiation force [34] and torque [35,36] we use the full scattering theory in the framework of the transition matrix (T-matrix) approach. In fact, this approach is quite general as it applies to particles of any shape and refractive index for any choice of the wavelength. Our starting point is the calculation of the field configuration in the focal region of a high numerical aperture (NA) objective lens in absence of any particle, using the procedure originally formulated by Richards and Wolf [37]. The resulting field is considered as the field incident on the particles, and the radiation force and torque exerted on any particle within the region is calculated by resorting to conservation of linear and angular momentum for the combined system of field and particles. As a result the optical force and torque exerted on a particle turn out to be given by the integrals [34,36]:

#117041 - $15.00 USD Received 11 Sep 2009; revised 19 Oct 2009; accepted 28 Oct 2009; published 6 Jan 2010

$$\mathbf{F}_{\mathrm{Rad}} = r^2 \int_{\Omega} \hat{\mathbf{r}} \cdot \langle \mathsf{T}_{\mathsf{M}} \rangle \, d\Omega \tag{1}$$

$$\mathbf{M}_{\mathrm{Rad}} = -r^3 \int_{\Omega} \hat{\mathbf{r}} \cdot \langle \mathsf{T}_{\mathsf{M}} \rangle \times \hat{\mathbf{r}} \, d\Omega \tag{2}$$

where the integration is over the full solid angle, r is the radius of a large (possibly infinite) sphere surrounding the particle centre, and $\langle \mathsf{T}_{\mathsf{M}} \rangle$ is the time averaged Maxwell stress tensor:

$$\langle \mathsf{T}_{\mathsf{M}} \rangle = \frac{1}{8\pi} \mathrm{Re}[n^2 \mathbf{E} \otimes \mathbf{E}^* + \mathbf{B} \otimes \mathbf{B}^* - \frac{1}{2}(n^2 |\mathbf{E}|^2 + |\mathbf{B}|^2)\mathrm{I}] \tag{3}$$

where $\otimes$ denotes dyadic product, I is the unit dyadic and n is the refractive index of the medium surrounding the particle. When the incident field is a polarized plane wave, the components of the radiation force along the direction of the unit vector $\hat{\mathbf{v}}_{\xi}$ are given by [34]:

$$\mathbf{F}_{\mathrm{Rad}\,\xi} = -\frac{r^2}{16\pi} \mathrm{Re} \int (\hat{\mathbf{r}} \cdot \hat{\mathbf{v}}_{\xi})[n^2 (|\mathbf{E}_{\mathrm{S}}|^2 + 2\mathbf{E}_{\mathrm{I}} \cdot \mathbf{E}_{\mathrm{S}}) + (|\mathbf{B}_{\mathrm{S}}|^2 + 2\mathbf{B}_{\mathrm{I}} \cdot \mathbf{B}_{\mathrm{S}})] \, d\Omega \tag{4}$$

where $\mathbf{E}_I$ and $\mathbf{B}_I$ are the incident fields, while $\mathbf{E}_S$ and $\mathbf{B}_S$ are the fields scattered by the particle. In turn the radiation torque takes on the form:

$$\mathbf{M}_{\mathrm{Rad}} = \frac{1}{8\pi} r^3 \, \mathrm{Re} \int n^2 \hat{\mathbf{r}} \cdot (\mathbf{E}_{\mathrm{I}} + \mathbf{E}_{\mathrm{S}})(\mathbf{E}_{\mathrm{I}} + \mathbf{E}_{\mathrm{S}}) \times \hat{\mathbf{r}} \, d\Omega \tag{5}$$

Expanding the incident field in a series of vector spherical harmonics with (known) amplitudes $W_{1\,lm}^{p}$, the scattered field can be expanded on the same basis with amplitudes $A_{l'm'}^{p'}$. The relation between the two amplitudes is given by $A_{l'm'}^{p'} = \sum_{plm} S_{l'm'lm}^{p'p} W_{1\,lm}^{p}$, where $S_{l'm'lm}^{p'p}$ is the T-matrix of the particle. In this framework, several kinds of non-spherical particles can be modeled as aggregates of spherical scatterers with size below the radiation wavelength. The elements of the T-matrix are calculated in a given frame of reference through the inversion of the matrix of the linear system obtained by imposing to the fields boundary conditions across each spherical surface [29]. Here we stress that each element of the T-matrix turns out to be independent both on the direction of propagation and on the polarization of the incident field. Thus they do not change when the incident field is a superposition of plane waves with different direction of propagation, i.e. for the description of a focused laser beam in the angular spectrum representation [38].

For polymer nanofibers, we calculate the radiation force ($\mathbf{F}_{rad}$) and torque ($\mathbf{M}_{rad}$) exerted by the optical tweezers, by modeling the nanostructures as linear chains of spheres with diameter, D, and length, L, equal to the fiber diameter and length, respectively. In Fig. 1(a)-1(b) we schematize the geometrical configuration of the system. In particular, the calculations of the torque can be obtained for any orientation of the polymer fiber and for different trapping positions.

#117041 - $15.00 USD Received 11 Sep 2009; revised 19 Oct 2009; accepted 28 Oct 2009; published 6 Jan 2010

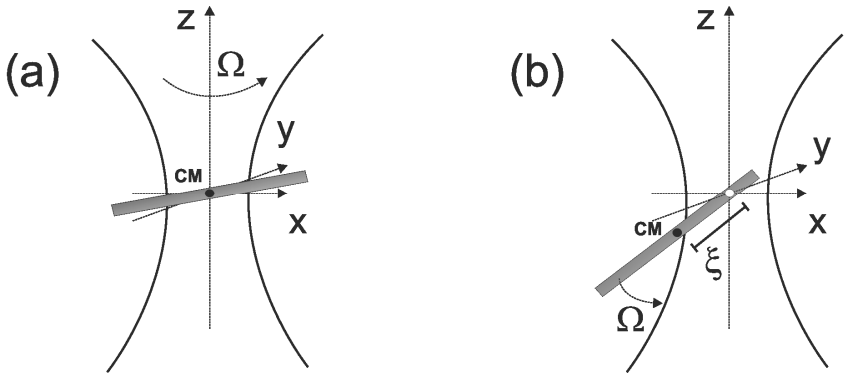

Fig. 1. (a) Sketch of the geometric configuration for a fiber trapped and rotated about its center-of-mass (black dot). Rotation occurs in the xy plane. (b) Geometry of the optical trapping of a fiber rotated about a point shifted by ξ towards the edge of the fiber (white dot).

2.2 Hydrodynamics

When dealing with quantitative comparisons between theory and experiments, a crucial issue to be addressed is the hydrodynamics of the trapped particle. For linear nanostructures (rigid rod-like structures), the viscous drag is described by an anisotropic hydrodynamic mobility tensor, whose components depend on the length of the linear structure (L) and on the length-to-diameter ratio, $p = L/D$ [39]. Symmetry considerations reduce the relevant hydrodynamics parameters to the translational, $\Gamma_{\perp}$ and $\Gamma_{\parallel}$, and rotational, Γ_{Rot}, mobilities [22], specifically when center-of-mass rotation is considered:

$$\Gamma_{\perp} = \frac{\ln p + \delta_{\perp}}{4\pi\eta L}, \quad \Gamma_{\parallel} = \frac{\ln p + \delta_{\parallel}}{2\pi\eta L}, \quad \Gamma_{Rot} = \frac{3(\ln p + \delta_{Rot})}{\pi\eta L^3} \tag{6}$$

where $\Gamma_{\perp}$ and $\Gamma_{\parallel}$ are the translational mobilities, transverse and parallel to the main axis respectively, Γ_{Rot} is the rotational mobility about the center-of-mass, where η is the dynamical viscosity of the surrounding medium, and δ_{Rot} represents end corrections, calculated as polynomial of $(\ln 2p)^{-1}$ [39]. On the other hand, when the pivot point of the rotation is shifted by a value ξ from the center-of-mass, we need to change L with $L+2\xi$ in the rotational mobility [Eq. (6)].

$$\Gamma_{Rot}(L+2\xi) = \frac{3(\ln \tilde{p} + \tilde{\delta}_{Rot})}{\pi\eta(L+2\xi)^3} \tag{7}$$

where $\tilde{p} = (L+2\xi)/D$ is an effective length-to-diameter ratio and $\tilde{\delta}_{Rot}$ is an effective end correction that takes into account the shift of the rotation pivot point with respect to the center-of-mass. For a rotating optically trapped polymer nanofiber, the radiation torque $\mathbf{M}_{rad}$ is counterbalanced by the hydrodynamic viscous torque (for the low Reynolds number regime) $\mathbf{M}_{hydro} = -\Omega/\Gamma_{Rot}\hat{\mathbf{n}}$ ($\hat{\mathbf{n}}$ is the rotation axis) and the fiber rotates at a constant rotation frequency:

$$\Omega = \left|\mathbf{M}_{rad}\right| \Gamma_{Rot}(L+2\xi) \tag{8}$$

that is dependent both on the length of the fiber and on the pivot point position. This relation holds when the fiber rotates in a plane orthogonal to the optical axis, i.e. for a situation

#117041 - $15.00 USD Received 11 Sep 2009; revised 19 Oct 2009; accepted 28 Oct 2009; published 6 Jan 2010

fulfilled in our experiments where the tilting angle is close to 90° i.e. $\sin\theta \approx 1$. Calculating the torque from our electromagnetic theory and Eq.s (7) and (8) yields the theoretical rotation frequency for the trapped fiber, directly comparable to experimental values.

3. Method

3.1 Realization of nanofibers

The polymeric nanofibers are fabricated by electrostatic spinning (ES) [40,41], exploiting a high electrostatic field (~0.9 kV cm^{-1}) to stretch a jet of polymer solution. Our samples are made by spinning a formic acid solution of poly(methylmethacrylate) (PMMA) with concentration of 26% (w/w). Due to the formic acid high conductivity and dielectric constant, the realization of uniform and beads-free fibers with a narrow size dispersion and diameters in the sub-micrometer range can be obtained. In a typical ES process, a 0.5 ml of PMMA solution is loaded into a 1.0 mL plastic syringe tipped with a 19-gauge stainless steel needle. The positive lead from a high voltage supply (XRM30P, Gamma High Voltage Research Inc., Ormond Beach, FL) is connected to the metal needle applying a bias of 9 kV. The solution is injected at the end of the needle at a constant rate of 10 μL/min by a syringe pump (33 Dual Syringe Pump, Harvard Apparatus Inc., Holliston, MA), which prevents dripping at the end of the metallic capillary. Fibers are collected as non-woven mat on an aluminum collector negatively biased at −2 kV and placed at a distance of 12 cm from the needle. All the ES experiments are performed at room temperature with air humidity about 40%. Finally, fibers are mechanically removed from the collector and stored in a vial containing distilled water. To allow the subsequent separation and fragmentation, the suspension of fibers in distilled water is sonicated for 1 hour at 25 °C before the trapping experiments.

3.2 Optical tweezers

Experimentally, our optical trap is custom-built on an inverted microscope (Zeiss Axiovert 40) as shown in Fig. 2(a), and based on a Ti:Sapphire laser (λ = 800 nm, Coherent). This is strongly focused to a diffraction-limited spot on the objective focal plane, by overfilling the back aperture of an oil-immersion infinity-corrected objective lens (100 × /1.3, Zeiss Plan-Neofluar) [42]. Bright field images and videos are recorded by a charge coupled device camera using the same objective lens as the trapping laser. The dispersed polymer nanofibers are placed in a sample cell comprises a poly(dimethylsiloxane) chamber in conformal contact with a glass cover slip, thus defining a 100 μL volume of the water suspension of fibers. The cover slip is mounted on a piezoelectric stage, allowing travelling over 300 μm along each axis with nanometric spatial resolution.

The dynamics and tracking of the polymer fibers is investigated by means of the back-scattered light from the same laser used to trap the sample. In particular, the applied torque is related to the rotation of the trapped nanofiber, characterized by measuring the time evolution of the back-scattered light. Collecting this light by imaging the back focal plane of the microscope objective onto a silicon quadrant detector provides a direct, non-contact method to measure the drag torque. Upon Fourier processing, the particle rotation frequency is recovered by the power spectrum density with high accuracy, and with larger bandwidth and better resolution than frame-by-frame video tracking [43].

#117041 - $15.00 USD Received 11 Sep 2009; revised 19 Oct 2009; accepted 28 Oct 2009; published 6 Jan 2010

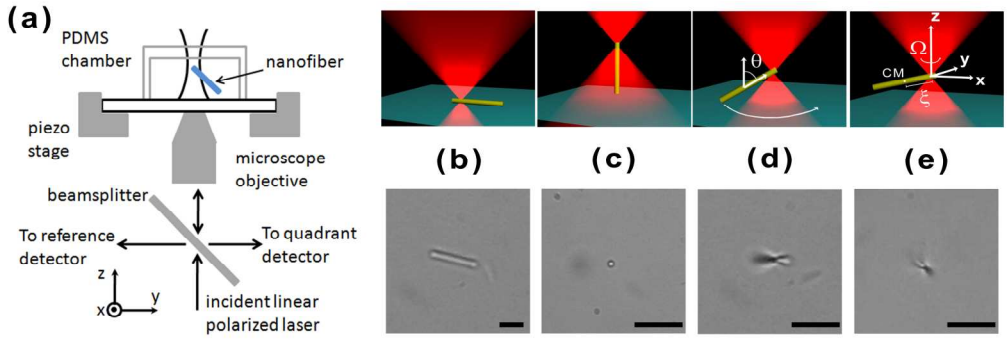

Fig. 2. (a) Scheme of the optical tweezers set-up with detection using backscattered light. The arrows indicate the light paths. (b)-(e): Optical rotation of the polymer fiber, schematized (top, Media 1), and imaged (bottom). The fiber main axis is tilted by θ from the optical axis, the trapping point is shifted by ξ from the center-of-mass (CM). Scale bar 2.5 μm.

4. Results and discussion

Figures 2(b)-(e) highlight the stages of fiber trapping and rotation. The particle is picked up from glass with low optical power [< 50 mW, Fig. 2(b)], and taken to a distance from the cover slip slightly larger than the fiber length. Once in this position the fiber stands upright, aligning its longitudinal axis to that of the optical axis of the laser beam [Fig. 2(c)]. We then increase the trapping power (100-400 mW) to confine the fiber in a stiff trap (Media 2). In this configuration we can translate the beam and the fiber along all the three axes. By approaching the cover slip to the fiber using the piezo-stage, the glass surface is led again in contact with the bottom tip of the fiber, which starts to tilt by an angle θ [Fig. 2(d)]. Above a critical angle depending on the trapping power, the fiber begins to rotate at constant rate (Ω) (Media 1). For some samples, we can also finally lower the piezo-stage, thus leaving the fiber not in contact with the glass surface while continuing to rotate in its tilted configuration [Fig. 2(e)]. This rotation mechanism is different from previously observed complex oscillations of tin oxide nanowires, attributed to the particle asymmetric cross-section shape [44].

In order to characterize the trapped fibers, we first test the alignment between the nanofiber and the polarization direction of the trapping beam for the configuration depicted in Fig. 2(d). To this aim we tilt the trapped cylindrical object near the surface, using low optical power and thus not causing any rotation, and we use a $\lambda/2$ plate to rotate the trapping beam polarization. The asymmetric backscattered light off the nanofiber is detected on the quadrant photodiode for each $\lambda/2$ plate angle, ψ. Upon decomposing the signal in top-bottom and left-right pairs, we determine the orientation angle of the new equilibrium position with respect to ψ. We find that the fiber aligns with the local polarization axis of the trapping field (Fig. 3), in agreement with previous results by Bishop et al. using glass rods (Media 3) [10]. Instead, with the trapped object pulled away from the cover slip, as schematized in Fig. 2(c), the fiber aligns along the optical axis, independently from the polarization, and no rotation is observed within the experimental error. Such lack of rotation for the fiber when aligned to the optical axis is an indication of the isotropy of the cylinder and end faces, as observed by scanning electron microscopy (SEM), Fig. 4(a) [18,19].

We then analyze the dynamics of tilted fibers by measuring the rotating frequency as a function of the incident optical power (Media 4). A time series of the quadrant photodetector signal over 20 s is used to determine the rotation frequency, from the frequency peak of the power spectrum [Fig. 4(b)]. Since only one sharp and symmetrical peak is detected along with its harmonics in the power spectral density, we conclude that the observed frequency is that of a continuous rotation of the fiber without nutation. We find that the rotation frequency increases linearly with the trapping power [linear fits through the origin shown in Fig. 4(c)],

#117041 - $15.00 USD Received 11 Sep 2009; revised 19 Oct 2009; accepted 28 Oct 2009; published 6 Jan 2010

which rules out the occurrence of nonlinear effects in the investigated experimental range. Moreover, Ω decreases upon increasing the fiber length, as expected from Eq. (8).

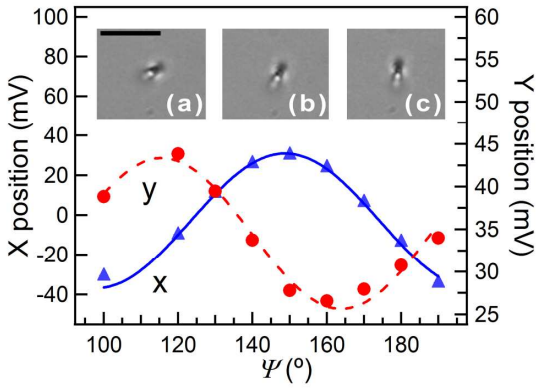

Fig. 3. Non-rotating tilted fiber aligning with external linear polarization vs. waveplate angle, ψ . Continuous line (blue) represents the x-axis position (left vertical scale), and the dashed line (red) the y-axis position (right vertical scale), projected onto the quadrant photodiode. Inset: Micrographs of a tilted nanofiber for ψ = 120° (a), 140° (b), and 160° (c). Scale bar = 5 µm.

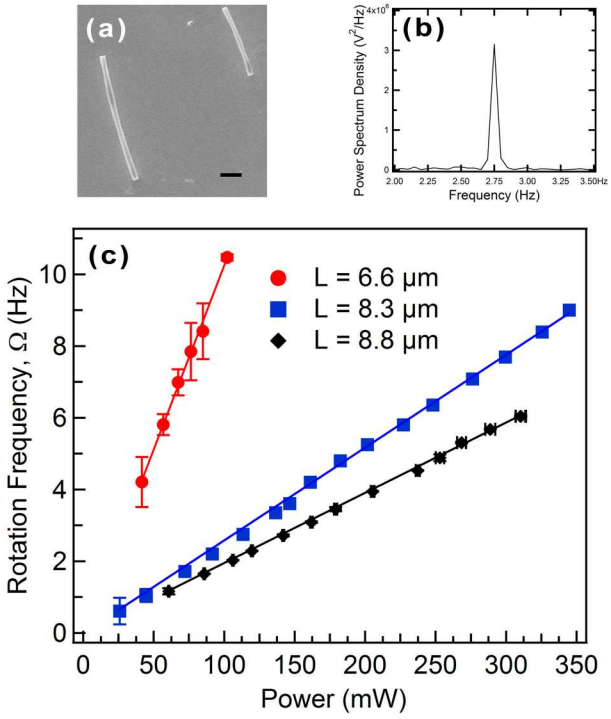

Fig. 4. (a) SEM of typical polymer fibers used in the rotation experiments, scale bar = 2 µm. (b) Typical peak of power spectral density corresponding to the rotating frequency of the trapped fiber (L = 8.3 µm) at optical power 113 mW. (c) Trapped rotating fiber frequency vs. trapping power, for fibers of different lengths, with their respective fits through the origin. Power values measured for light before entering the microscope.

#117041 - $15.00 USD Received 11 Sep 2009; revised 19 Oct 2009; accepted 28 Oct 2009; published 6 Jan 2010

Finally, we investigate the dependence of the rotation frequency on the tilting angle (θ). To this aim, we keep the rotating fiber at a constant power (115 mW) and vary the fiber-to-cover slip distance using the piezo-stage at sub-micron intervals. The angle θ is calculated from the fiber length and the fiber-to-cover slip distance. In Fig. 5, we display the rotation frequency vs. $\sin\theta$. The rotation frequency is almost constant for angles up to 82° ($\sin\theta$ = 0.99) and the calculated frequencies, based on a model of a rotating fiber around its end-point ($\xi \approx L/2$), well describe the measured values. An increase of the rotation frequency is observed for angles approaching $\sin\theta$ = 1, an effect that is not related to the increasing tilt, that would cause a decrease of the rotating frequency if the pivot point is unchanged (Fig. 5). We attribute the increase of the rotation frequency for high tilt angles to a progressive shift of the trapping point from the fiber tip towards the fiber center-of-mass. In fact, our calculation reproduces quite well the experimental results when assuming a progressive shift of the trapping point from the fiber tip towards its center-of-mass mass (up to $\xi \approx L/4$). Recently reported analytical calculations of radiation torque exerted on a spheroid, but with the trap centered on the spheroid, exhibit a similar behavior for high tilt angles [45].

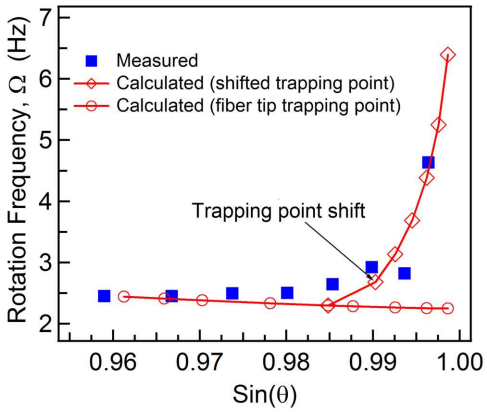

Fig. 5. Comparison of the measured (full blue squares) and calculated (empty red circles and empty red diamonds) trapping frequency vs. sine of the tilt angle, θ, for a fiber with length L = 8.8 μm. The rotation frequencies are calculated by assuming a trapping point close to the fiber tip (empty red circles) or a progressive shift towards the fiber center of mass (empty red diamond). The shift between two consecutive calculated points is of 0.45 μm.

5. Conclusions

We demonstrated optical trapping and manipulation of polymer nanofibers, introducing the control of rotation over these elongated nanostructures by tilting the trapped fiber. The measured rotation frequencies in the different trapping configurations agree with calculations based on a T-Matrix formalism for optical force and torque. The manipulation of these novel nanomaterials hold promises for many applications, such as photonic circuits or microfluidics, that can benefit from the controlled manipulation and rotation of the nanofibers, and the assembly of active polymeric fibers in ordered arrays. In particular the control over length and size makes polymer nanofibers ideal probes in next generation Photonic Force Microscopy.

Acknowledgments

This work was partially supported by the Italian Minister of University and Research through the FIRB programs RBIN045NMB and RBIP06SH3W, and by the Apulia Regional Strategic Project PS_144. The authors gratefully acknowledge R. Stabile for the SEM images.

#117041 - $15.00 USD Received 11 Sep 2009; revised 19 Oct 2009; accepted 28 Oct 2009; published 6 Jan 2010